

The Relationship Between Mixed Rossby-Gravity Waves and Convection in a General Circulation Model

By Peter G. Hess

National Center for Atmospheric Research, Boulder, Colorado, U.S.A.

Harry H. Hendon

Center for Atmospheric Theory and Analysis, University of Colorado, Boulder, Colorado, U.S.A.

and

David S. Battisti

Department of Atmospheric Sciences, University of Washington, Seattle WA, U.S.A.

(Manuscript received 13 August 1992, in revised form 28 January 1993)

Abstract

We investigate the relationship between mixed Rossby-gravity waves (MRGWs) and convection in a general circulation model. The experiments described are performed in a general circulation model with the lower boundary set to that of an ocean surface everywhere. Several experiments are run varying the convective parameterization scheme (using either a modified Kuo scheme or a moist convective adjustment scheme) and varying the tropical sea surface temperatures (specified to be zonally symmetric in all cases), thereby changing the location of the modeled intertropical convergence zones (ITCZs). The appearance of a robust MRGW occurs when the sea surface temperature is such that two ITCZs straddle the equator. The particular sea surface temperature distribution used and the parameterization scheme for convection also affect the structure and strength of the modeled MRGW. The vertical structure of MRGWs is analyzed in the experiment in which this wave mode is the most energetic. We show that MRGWs of several different zonal length scales exist in the troposphere in association with convection; however, it is only the longer length scales which can be discerned in the upper troposphere and lower stratosphere.

1. Introduction

Waves with a four to five day period are ubiquitous in the tropics. These waves include the easterly waves observed over the Pacific and Atlantic basins as well as both upper and lower tropospheric mixed Rossby-gravity waves (MRGWs). In this frequency range there is a large peak in the cloud brightness spectrum (Zangvil and Yanai, 1981), in the outgoing longwave radiation (OLR) and in the brightness temperature (Salby *et al.*, 1991), especially in the region of the intertropical convergence zone (ITCZ). Salby *et al.* (1991) attribute much of this brightness variance to easterly waves (Reed and Recker, 1971). MRGWs also contribute to the prominent 4 day peak in the brightness spectrum. Hendon and Liebmann (1991) (HL) demonstrate that an OLR signal,

antisymmetric about the equator in the central Pacific, is associated with MRGWs in the lower troposphere with periods of 4 days. This is consistent with Salby *et al.* (1991) who find that the brightness temperature signal tends to be anti-correlated across the equator during the occurrence of double ITCZs.

Early analysis of station data in the equatorial Pacific indicates disturbances with wavelengths ranging between approximately 3000 and 10000 km with periods of 4–5 days (see Wallace, 1971, for a review of this early work). As discussed by Wallace (1971) the shorter wavelength modes, generally with maximum amplitude in the meridional wind between 5° and 10° latitude and prominent at the western Pacific stations, are distinct from the modes with longer wavelengths and with maximum amplitude on the equator. A wave found across the Pacific

in the lower stratosphere, discovered by Yanai and Maruyama (1966) and often referred to as the Yanai wave is identified with a MRGW mode of wavelength 10000 km. Reports of fluctuations in the meridional wind in the lower troposphere with wavelengths between 8000 and 10000 km (wavenumbers 4 and 5) are documented from station data over the central equatorial Pacific (Nitta, 1970; Yanai and Maruyama, 1970).

Using the analysis product from ECMWF, Liebmann and Hendon (1990) (LH) show a broad peak in the power of the equatorial meridional wind at 850 mb in the Pacific basin for westward moving disturbances in the 3.5–6 day band and wavenumbers 4–8. In the central Pacific a regression about the 850 mb equatorial meridional wind gives a wavenumber of about 6 or 7, with a structure and dispersion relationship consistent with equatorially trapped MRGWs (LH). This wave is unambiguously correlated with OLR anomalies. The relation of this wave to the upper tropospheric Yanai wave has not been firmly established, nor the relation of the Yanai wave to clouds.

While the tropospheric MRGW contributes to the large 4 day peak in the brightness spectrum, the MRGW in the lower stratosphere is thought to be important in forcing the easterly phase of the stratospheric quasi-biennial oscillation (QBO). Absorption of this wave induces a westward acceleration to the lower stratospheric winds when the mean wind shear is easterly, thus causing a descent of the zonal mean easterlies (Lindzen and Holton, 1968; Holton and Lindzen, 1972).

The forcing mechanism for MRGWs is still speculative. Hayashi (1970) finds that parameterizing the heating with a CISK type parameterization destabilizes the neutral equatorial modes. The three dimensional structure of the resulting destabilized MRGW agrees very well with the observed structure. In particular, the southwest (northwest) to northeast (southeast) tilt of the wave in the northern hemisphere (southern hemisphere) and the vertical phase structure is consistent between theory and observations. Although Hayashi shows the unstable MRGW is preferred over the Rossby wave modes, he cannot explain the frequency or wavelength of the observed waves: the instability analysis favors longer wavelengths and shorter periods than those observed. Kuo (1975) argues that the preferred spatial and temporal scales of the most unstable CISK equatorial modes are consistent with observed wave characteristics if waves with sufficiently short periods cannot supply water fast enough to sustain an instability through the CISK mechanism. Numerical experiments with a primitive equation β -plane model (Itoh and Ghil, 1988) support the conclusion that the phase speed associated with the longer westward propagating MRGWs is too fast to effec-

tively excite wave-CISK.

The model results of Holton (1974) indicate that equatorially antisymmetric heating with a 5 day period effectively generates MRGWs. Salby and Garcia (1987) (SG) demonstrate with linear theory the sensitivity of the equatorially trapped modes to the three dimensional structure of stochastic heating. In particular, the amplitude of the response of a particular wave mode (with fixed length and time scales) to the heating is given by the projection of the heating, prescribed in time and space, onto the Hough mode in question. The projection is particularly strong if the heating spectrum is white because the response to heating scales by the inverse of the wave frequency. A white heating spectrum allows efficient projections onto the fairly high frequency MRGW. SG show that a stochastic distribution of heating, defined by given spectral characteristics, can produce weak MRGWs when the heating is located to the north of the equator (they did not study the case governed by the stochastic heating generated in both hemispheres by a double ITCZ). However, their analysis is linear and does not account for the stability of the wave solution or the feedback of the forced wave on the heating field.

Recently, HL show that in the central Pacific the lower tropospheric wave amplitude of the MRGW is strongly peaked during the boreal fall season, coinciding both spatially and temporally with a region where the sea surface temperature (SST) reaches values greater than 28° on both sides of the equator. This SST distribution favors convection located off the equator in both the northern hemisphere (N.H.) and southern hemisphere (S.H.). In fact, during the fall months in the central Pacific two ITCZs are often observed straddling the equator. Moreover, the power of OLR antisymmetric about the equator is almost three times the symmetric power (HL). The coincidence of MRGW modes with equatorially symmetric SSTs and equatorially antisymmetric heating suggests a strong relationship between SST, the location of convection and the occurrence of MRGWs (HL).

The fact that the peak amplitude of this wave occurs during the equinoctial seasons suggests that the primary forcing mechanism for lower tropospheric MRGWs is not from mid-latitude disturbances as postulated by Itoh and Ghil (1988)¹. Randel (1992) also stresses the importance of lateral forcing, coupled with near zero or easterly winds at the equator in forcing an apparent MRGW in the upper troposphere². Randel finds very little evidence of a

¹Itoh and Ghil are lead to predict the maximum power of MRGWs occurs during solstitial seasons when the equatorially asymmetric component of the mid-latitude forcing is largest.

²Randel (1992) identifies a wave in the upper troposphere over the eastern Pacific with a period between 6 and 10 days

Table 1. The experiments are identified in the left hand column. The case is identified first by the type of convective scheme, either Kuo or moist convective adjustment (MCA), and then by the lower boundary sea surface temperature condition. The second column indicates the location of ITCZ(s) for each model run. The average precipitation (mm/day) within each ITCZ is found in column three. Finally the maximum sea surface temperature is given in column 4. The SST distributions used are summarized here: *Std*: The standard SST distribution. SST is symmetric about the equator with maximum SST on the equator. This distribution is the observed SST distribution for March 21, zonally averaged and symmetrized about the equator. *Peq*: A strongly peaked symmetric SST distribution, with a marked SST maximum on the equator. The maximum SST is as in the standard case. *Poeq*: As in the Peq case, but with the peak in the SST located in the Northern Hemisphere at 10°N. *Feb*: SST is asymmetric about the equator with maximum temperature in the Southern Hemisphere. It is representative of the climatological February temperatures in the central Pacific, but the equatorial asymmetry has been further emphasized. *Oct*: The SST is the symmetrized climatological October SSTs in the central Pacific, which features a SST minimum on the equator.

CASE	ITCZ LOCATION		PRECIPITATION (mm/day)		MAXIMUM SST (K)
	S.H.	N.H.	S.H.	N.H.	
Kuo-Feb	13.5°	7°	12.5	8.0	302.7
Kuo-Oct	7°	7°	10.7	10.2	302.0
MCA-Oct	7°	7°	7.4	8.0	302.0
Kuo-Std	4-7°	4-7°	8.3	8.7	301.0
MCA-Std	Eq.		14.6		301.0
Kuo-Poeq	10°N		17.5		301.0
Kuo-Peq	Eq.		19.0		301.0

connection between this wave mode and lower tropospheric forcing by convection. Hayashi (1974) documents a 4-5 day peak in the meridional wind in the lower stratosphere, corresponding to a MRGW of wavenumber 4 in the GFDL general circulation model. He finds very little relation, however, between the space-time distribution of tropospheric convective sources and this MRGW.

In this paper we will concentrate on the convective activity associated with the equatorially trapped tropospheric MRGW in a general circulation model (GCM). We show the relation between this tropospheric wave mode and the MRGW observed in the lower stratosphere. We find, consistent with the hypothesis proposed by HL, that the robust presence of the MRGW coincides with the presence of two ITCZs straddling the equator. The paper proceeds as follows. Section 2 gives a brief description of the model and the experimental setup. Section 3 documents the horizontal and vertical structure of the MRGW mode in the model experiment in which it is the most pronounced and examines the relationship between the MRGW observed in the lower troposphere and that observed in the upper troposphere/lower stratosphere. Section 4 examines the sensitivity of the MRGW to the number and location of the ITCZs, as well as to the SST and con-

and a wavenumber between 4 and 7. This wave has the horizontal structure of a MRGW, although it is not necessarily centered over the equator. It is evidently distinct from the 4-5 day MRGW mode.

vective scheme. Section 5 gives our conclusions.

2. Description of experiment

All experiments are performed with an aquaplanet version of the NCAR Community Climate Model (Version 1) (CCM1) with T42 resolution and a vertical grid of 12 levels. The sigma values of the 12 levels are 0.991, 0.926, 0.811, 0.664, 0.500, 0.355, 0.245, 0.165, 0.110, 0.060, 0.025 and 0.009. Simple bulk aerodynamic parameterizations of surface exchange, and subgrid-scale vertical diffusion are used (Deardorff, 1972). Large-scale stable condensation, parameterized convection and radiatively active clouds are included in this model. For further information on the CCM1 see Williamson *et al.* (1987).

All experiments run are at least 80 days in length. They are run in a perpetual March 21 simulation, so that the sun is situated directly over the equator. The diurnal cycle is not simulated. The lower boundary condition for these runs is that of a sea surface, where the temperature has been fixed at a value independent of longitude. The experiments are performed with either a moist convective adjustment (MCA) cumulus parameterization scheme (following Manabe *et al.*, 1965), or a modified Kuo type convective parameterization [derived from Kuo (1965, 1974), Anthes (1977), Donner *et al.* (1982), Donner (1986) and Krishnamurti *et al.* (1983)]. Further information on these convective parameteriza-

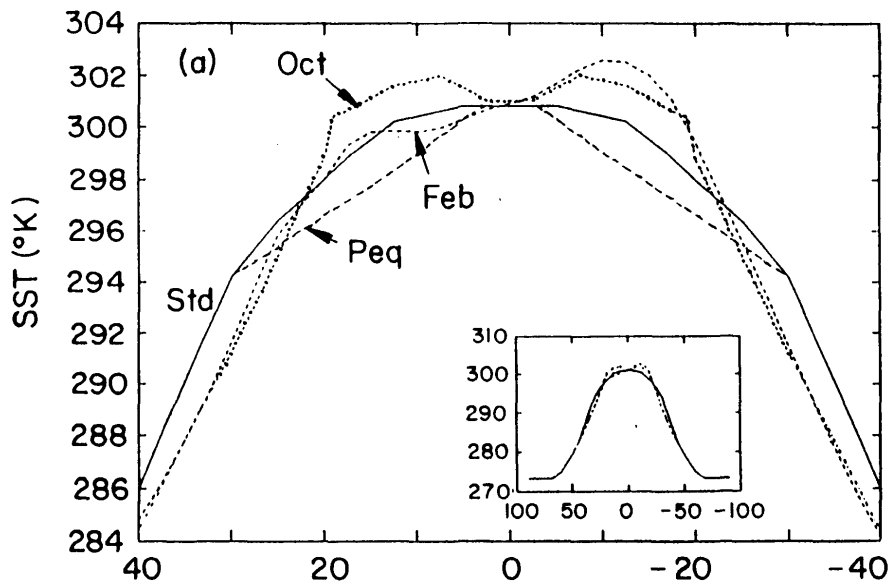


Fig. 1. The prescribed meridional distribution of sea surface temperature vs. latitude for various experiments. The Standard SST distribution (“Std”, solid line), February (“Feb”, short dashed line), October (“Oct”, dotted line) and peaked (“Peq”, long dashed line) sea surface temperature distributions are shown.

tions as well as the version of the model used in this study is given in Hess *et al.* (1993) (HBR).

Each experiment discussed below can be labeled by the type of convective scheme used (either Kuo or MCA) and by the SST distribution used (see Table 1). Five zonally symmetric SST distributions are used, referred to as: Std, Oct, Feb, Peq and Peoq. Four of these distributions are shown in Fig. 1. The standard SST distribution (“Std”) uses the observed zonally averaged SST for March 21, symmetrized about the equator, with the SST modified near the poles so temperatures remain above freezing. The maximum SST is on the equator in this case. The “Feb” SST profile is similar to the climatological February temperatures in the central Pacific Ocean, characterized by an asymmetric SST profile about the equator, with the maximum SST located at 10°S (the climatological hemispheric asymmetry in the February SST has been over-emphasized in the “Feb” SST profile given here). The “Oct” SST resembles the climatological October SST of the central Pacific and features a slight SST minimum on the equator, with SST maximums located near 10°N and 10°S. The SST distribution noted by “Peq” is sharply peaked with the maximum SST located on the equator, while “Poeq” (not shown) is similar to the “Peq” case, except it has the strongly peaked SST maximum located at 10°N.

The location of the ITCZ is sensitive to both the SST and to the convective parameterization scheme used (HBR). It is evident from the Table 1 that two ITCZs are obtained using the Kuo scheme except in the case where the ITCZ is sharply peaked (Poeq,

Peq). In the moist convective adjustment scheme a double ITCZ only occurs when the model SST resembles the October SST in the central Pacific.

3. Modeled mixed Rossby-gravity waves

In this section we examine the structure of the MRGW in the CCM1, then discuss the observed structure from a theoretical viewpoint. We concentrate on the Kuo-Oct case, as it is this experiment which produces the most power in the MRGW mode. In this experiment a double ITCZ is produced over the warmest water (see Table 1). In (3.1) we examine the horizontal structure of the MRGW in the lower troposphere and document that the CCM1 produces a mode very similar to that found by LH, then we examine the vertical structure of this wave and the relationship between the lower tropospheric wave mode and the upper tropospheric/lower stratospheric wave. The coarse vertical resolution above the lower stratosphere suggests the use of caution in the interpretation of the results above approximately 20 km. In (3.2) we discuss the wavenumber selection of the MRGW due to the zonal mean wind in the upper troposphere and lower stratosphere.

3.1 Structure of the modeled mixed Rossby-gravity wave

The distinctive signature of a MRGW is a meridional wind that is strongest on and symmetric about the equator (Matsuno, 1966). [The MRGW is distinct from the easterly wave which is localized off the equator and has eastward phase speeds with respect to the advecting wind (see, *e.g.*, Reed and

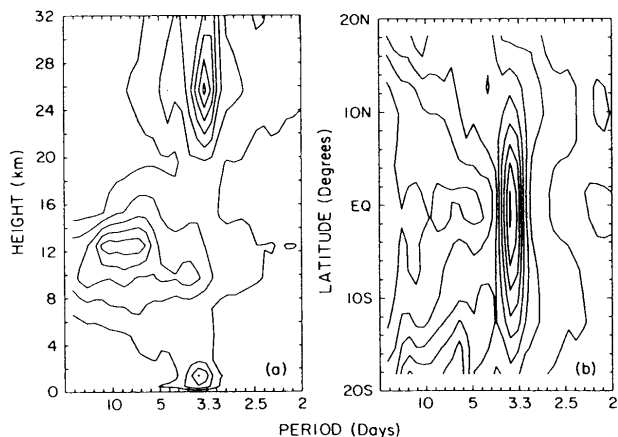


Fig. 2. Sections of the power of the equatorially symmetric component of the meridional wind for the Kuo-Oct case based on daily data for 64 days. a) Height-period section of the symmetric meridional wind. The contour interval is .1 $m^2/sec^2/spectral\ estimate$. b) Latitude-period section of the symmetric meridional wind at 811 mb. The contour interval is .05 $m^2/sec^2/spectral\ estimate$.

Recker, 1971).] The power of the equatorial symmetric meridional wind (the symmetric meridional wind is defined as: $[v(1.4^\circ) + v(-1.4^\circ)]/2$, where v is the meridional wind) in the 2.5–5 day range reaches maximum amplitude in the lower troposphere, in the upper troposphere and again in the lower stratosphere, with apparent nodes in the power near 5 and 18 km (Fig. 2a). The distribution of power in this diagram agrees qualitatively with that obtained in the modeling study of Hayashi (1974) and with the observational study by Yanai and Murakami (1970). The latter paper shows power spectra of the meridional wind at equatorial stations with the maximum power between 4 and 5 days near 2 km, 10 km and 16 km; nodes in the power occur between these heights. We note from Fig. 2a that in the upper troposphere much of the power is at periods greater than 5 days. Upper tropospheric waves with periods between 6 and 10 days have recently been investigated by Randel (1992). Fig. 2b documents that the peak in the power of the symmetric meridional wind at 811 mb (1.4 km) in Fig. 2a is indeed centered on and symmetric about the equator. The sharp peak near 3.6 days in the power of the meridional wind is similar to observations over the central pacific at 850 mb (HL) and is consistent with the expected structure of a MRGW.

Figures 3a and 3b show the distribution of power for the equatorially symmetric meridional wind at 811 mb (1.4 km) and equatorially antisymmetric rainfall (defined as $[P(7^\circ) - P(-7^\circ)]/2$, where

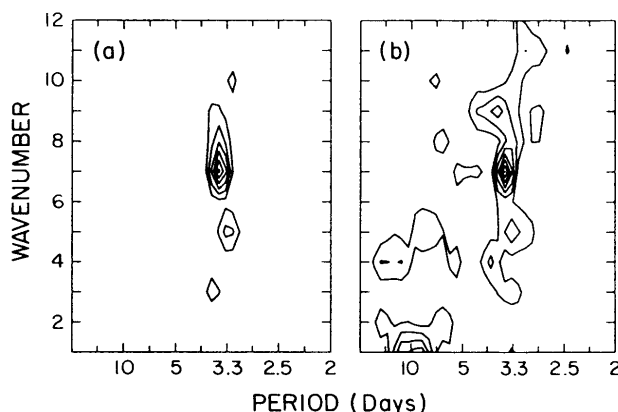


Fig. 3. The wavenumber versus period spectra for westward moving disturbances for the Kuo-Oct case at 811 mb, based on daily data for a 75 day time series. a) The symmetric component of the meridional wind about the equator at 811 mb. The contour interval is .025 $m^2/sec^2/spectral\ estimate$. b) The antisymmetric component of rainfall about the equator. The contour interval is .06 $mm^2/day^2/spectral\ estimate$.

P is the precipitation) for westward moving disturbances. At 811 mb the maximum power in the symmetric meridional wind occurs at wavenumber 7 (with secondary maxima at wavenumbers 5 and 3) and a period near 3.6 days. The power in antisymmetric rainfall coincides (Fig. 3b) to a large extent with the power for the equatorially symmetric 811 mb meridional wind, with maxima at wavenumbers 7, 5 and 3. It is not surprising that the cloud distribution is highly correlated with the lower tropospheric wave disturbance at wavenumber 7 (not shown).

A Hoffmüller plot of the symmetric meridional wind on the equator is shown in Fig. 4 for the Kuo-Oct case at 811 mb. The symmetric meridional wind has been processed using a band pass filter (Murakami, 1979) with half power at 2.5 and 5 days. The westward propagation of the meridional wind component on the equator is evident. It is clear from Fig. 4 that regions of strong meridional winds with westward phase propagation tend to occur sporadically in “packets”, with nearly stationary group propagation. This stationarity has also been noted by Wallace (1971) using observations of clouds. The packets tend to be strongly localized about adjacent longitudes, extending approximately one wavelength in width, and amplify and decay over a timescale of about 10 to 15 days. The mechanism for this slow timescale growth and decay is not known.

The coexistence of several temporal and spatial scales for westward propagating disturbances can be seen in Fig. 4 (and is suggested by Fig. 3). The dis-

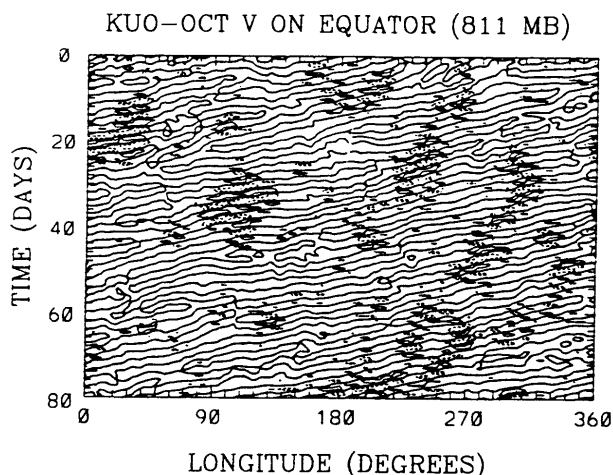


Fig. 4. Hoffmüller plot of the time filtered symmetric meridional wind at 811 mb on the equator between 0 and 80 days and from 0° to 360° for the Kuo-Oct case. The contour interval is 3 ms⁻¹. Positive contours are solid, negative contours are dashed. The time filter has half power at 2.5 and 5 days.

turbance centered near 235° day 25 has a period of about 3.6 days, a zonal wavenumber near 8 and a westward phase speed of 15 m s⁻¹. The disturbance located near 110° at 33 days has the same period, but is between wavenumber 4 and 5 and has a phase

speed of 29 m s⁻¹. These two scales are in agreement with the various length scales of MRGWs observed in the lower troposphere.

The structure of the 2.5–5 day wave is depicted clearly by regression analysis. The geopotential heights, wind and rainfall are regressed onto the symmetric meridional wind at 811 mb for the Kuo-Oct case (Fig. 5). All fields are band pass filtered (from 2.5 to 5 days) in this regression, and in all subsequent regressions. The features shown in this figure are highly statistically significant and have the characteristics of a MRGW (Matsuno, 1966): the geopotential height field, zonal velocity and rainfall are antisymmetric about the equator, the meridional wind is symmetric about the equator and maximizes on the equator. The wave in this regression resembles that obtained by LH (their Fig. 12) using the ECMWF analyses product and a base regression about a point over the central Pacific at 850 mb, where OLR is used as a proxy for rainfall. Both figures show the geopotential height maxima (minima) to be located in the vicinity of 10° latitude with a southwest (northwest) to northeast (southeast) tilt of the geopotential height fields in the N.H. (S.H.). The rainfall maximum in the model and the OLR minimum in the data also exhibit a southwest to northeast tilt in the N.H., with the maximum rainfall (minimum OLR) displaced towards low pressure from the maximum convergence of the wind at 811 mb. The displacement of the rainfall from the con-

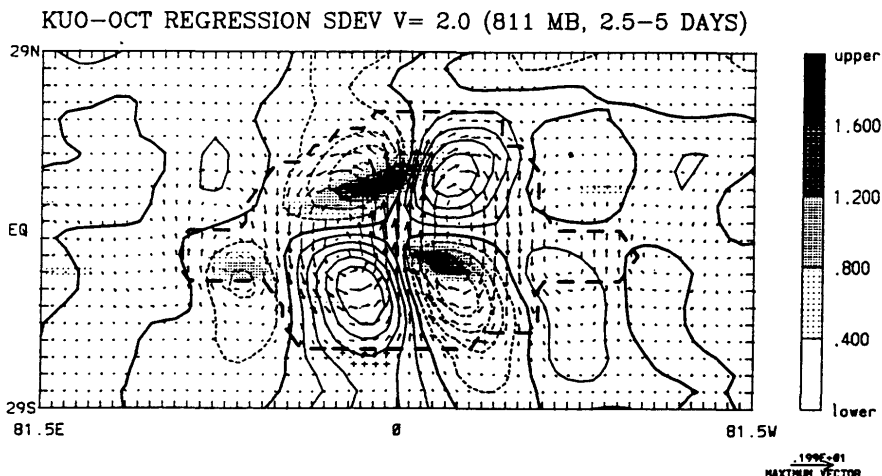


Fig. 5. Latitude, longitude section of a zonally averaged linear regression analysis performed at each longitude point at 811 mb between the symmetric meridional wind on the equator and the anomaly vector winds (arrows), geopotential heights (contours) and rainfall (shading). The fields represent anomaly fields bandpass filtered, with half power at 2.5 and 5 days. The contour interval for the geopotential is .2 m, negative contours are dashed, positive contours solid and the heavy contour is the zero contour. The rainfall is in mm/day and the wind fields are in ms⁻¹. All fields are scaled to the standard deviation of the meridional wind symmetric about the equator: 2 ms⁻¹. Within the heavy dashed line the winds are significant at the 95 % level. Outside of the region of significant winds the 95 % significance for the geopotential height is marked by '+'. The significance is computed using a Student-t test, assuming 16 independent longitudinal points (assuming every 8 points are independent) and 20 independent time samples (assuming every 3.5 days are independent).

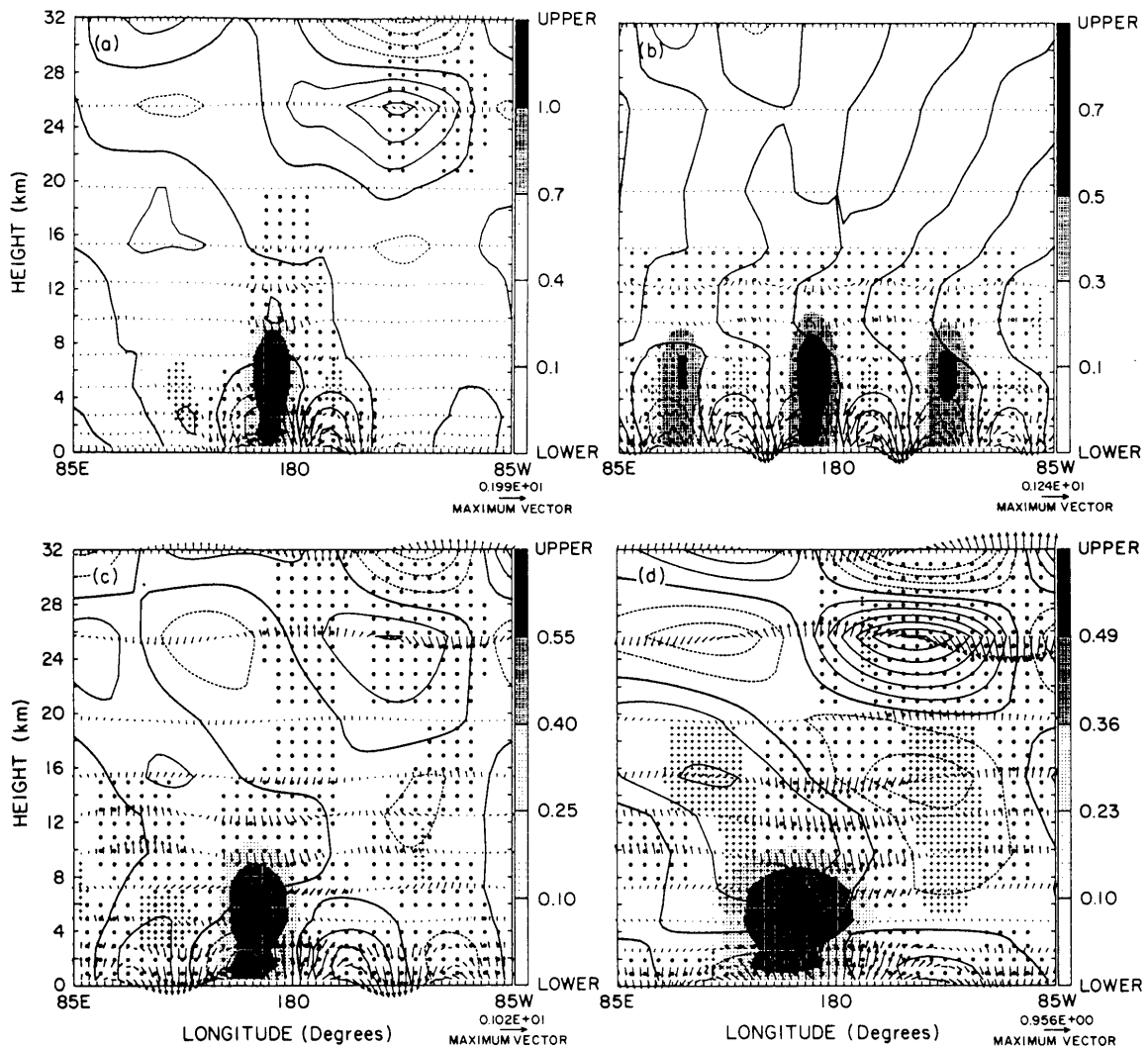


Fig. 6. Height, longitude section of a zonally averaged linear regression analysis performed at each longitude point between the 811 mb symmetric meridional wind on the equator and the following: the anomaly vector winds (arrows), antisymmetric geopotential heights (10°N minus that at 10°S) (contours) and antisymmetric latent heating (7°N minus that at 7°S) (shading, with scale given on the right). The longitudinal component of the vector wind field is given by the regression with the antisymmetric component of the zonal wind field (10°N minus that at 10°S); the vertical component is given by the regression with the equatorially symmetric component of the meridional wind. (Thus, the vectors give an indication of the strength and the phase of the wind field). The fields represent anomaly fields bandpass filtered with half power at 2.5 and 5 days, scaled by the standard deviation of the meridional wind symmetric about the equator (v_{sdv}). a) No spatial filtering, $v_{sdv} = 2 \text{ ms}^{-1}$; b) fields are spatially filtered between wavenumbers 6 and 8, $v_{sdv} = 1.2 \text{ ms}^{-1}$; c) fields are spatially filtered between wavenumbers 3 and 5, $v_{sdv} = 1 \text{ ms}^{-1}$; d) fields are spatially filtered between wavenumbers 1 and 3, $v_{sdv} = .96 \text{ ms}^{-1}$. The contour interval for the geopotential is .3 m, negative contours are dashed, positive contours are solid, and the heavy contour is the zero contour. The heating is in degrees/day and the wind fields in ms^{-1} . Note different intervals for the heating in each section. Regions of significant winds at the 95 % level are indicated by 'o', regions of significant geopotential outside of the region of significant winds are marked by '+'. The significance is computed as in Fig. 5, but based on 7, 5 and 3 spatial degrees of freedom respectively for parts (b), (c) and (d).

vergence at 811 mb, towards low pressure, is probably a consequence of the fact that the low level boundary layer boundary layer convergence is displaced towards low pressure in moist MRGWs (e.g.,

Holton *et al.*, 1971). The wavelength of the MRGW is estimated to be about 5600 km in the model data, corresponding to a wavenumber of about 7. The regressed wavelength is heavily weighted towards

the predominant scale of the MRGW and is slightly shorter than that in the central Pacific during the boreal fall (LH), also estimated using a regression analysis. In summary, the CCM1 successfully reproduces the horizontal structure of the MRGW observed by LH in the Kuo-Oct case.

We proceed to examine the vertical structure of this wave mode. Figure 6a shows the results of a regression of the symmetric meridional wind at 811 mb and the heating, geopotential anomalies and wind at other levels: see the caption for an explanation of this figure. The phase relationships depicted are consistent with those expected for MRGWs at all altitudes: the symmetric component of the meridional wind is 90° out of phase with the antisymmetric components of geopotential height, heating and zonal wind. A horizontal regression analysis at 25 mb (25.8 km) (not shown) indicates that the horizontal structure of the disturbance is consistent with that of a MRGW; the case is not so clear for the disturbance located at 245 mb (9.8 km) in Fig. 6a. The features shown are highly statistically significant in the vicinity of the heating in the lower troposphere, as well as to the east of the heating in the lower stratosphere. The strongest heating occurs just to the west of the regression point with weak heating signatures also occurring further to the east and to the west. In the vicinity of the heating the regression indicates a pronounced baroclinic structure within the troposphere, with a reversal of phase near the heating maximum. Away from the heating maximum the regressed wave tilts only slightly within the troposphere: the eastward tilt of the MRGW obtained by LH within the troposphere is not readily observed. Above the heating maximum the modeled MRGW exhibits a strong westward tilt in geopotential height, indicative of an upwards propagating mode. At 26 km and above the vertical structure of the disturbance is probably influenced by the upper model boundary. The group propagation appears to be upward and eastward in agreement with that expected for a MRGW and consistent with a low level energy source.

One of the most striking features of the regression shown in Fig. 6a are the different length scales of the oscillations in the winds and geopotential height between the lower troposphere and the upper troposphere/lower stratosphere. The apparent zonal length scale of the MRGW appears to increase rapidly with increasing height. Height-longitude regressions spatially filtered from wavenumbers 6–8, wavenumbers 3–5 and wavenumbers 1–3 are shown in Fig. 6b, 6c and 6d. In the lower troposphere the heating projects onto each of these zonal wave modes in a manner consistent with that expected from the low level convergence associated with MRGWs: the antisymmetric heating is located just to the west of the maximum meridional velocity within

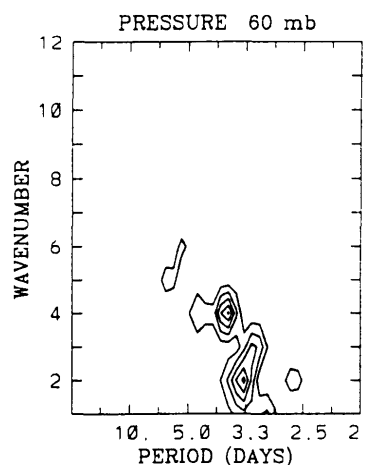


Fig. 7. As in Fig. 3a, but at 60 mb. The contour interval is $.015 \text{ m}^2/\text{sec}^2/\text{spectral estimate}$.

the low geopotential anomaly. The heating anomalies strongly project onto the geopotential height anomalies at all wavelengths, despite the fact that the precipitation (and the heating) occur primarily at wavenumber 7 (Fig. 3). This suggests that the convective heating is fundamental to the maintenance of all wavelength MRGWs, irregardless of the scale of the modes. It is immediately apparent from this figure that while the wavenumber 3–5 and wavenumber 1–3 lower tropospheric wave components have upper tropospheric and lower stratospheric counterparts, the wavenumber 6–8 components are confined to the lower and middle troposphere.

The shift of power towards longer length scales above the tropopause is confirmed in Fig. 7 (compare with Fig. 3), which shows the power of the symmetric meridional wind as a function of period and wavenumber for westward moving disturbances at 60 mb (19.6 km), a level located above the convective heating. At this height most of the power is shared between wavenumber 4 and wavenumber 2. A wavenumber of 4 is in agreement with that of the longer wavelength MRGW mode, often referred to as the Yanai wave (Yanai and Maruyama, 1966), observed in the upper troposphere and lower stratosphere. At 25 mb (25.7 km) the power is dominated by wavenumber 2 (not shown). The power at wavenumber 7 is not visible above 15 km. The power of the symmetric meridional wind for wavenumbers 7, 4 and 2 is shown as a function of height in Fig. 8. In the lower troposphere the response maximizes, near 3.6 days in each case, as expected from the association of each wave mode with convection, documented above. For the wavenumber 4 and wavenumber 2 modes there is also considerable response in the upper troposphere and lower stratosphere, with very little shift in frequency between

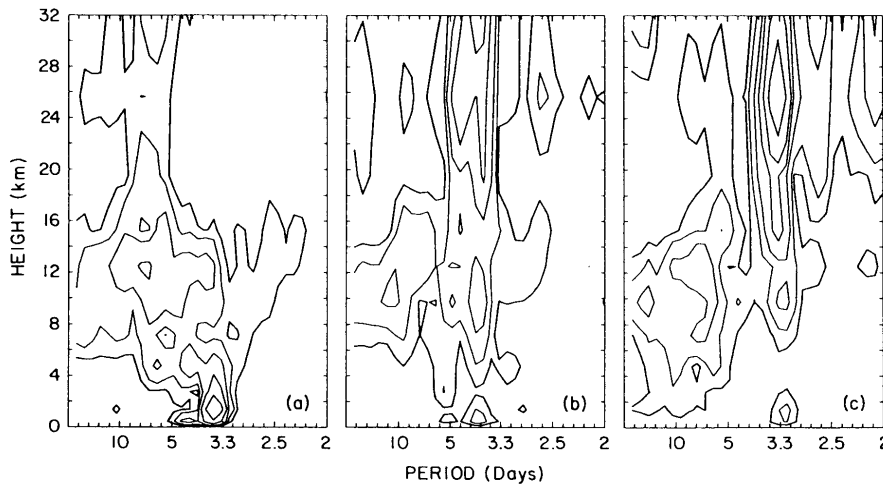


Fig. 8. As in Fig. 2a, but for the symmetric meridional wind spatially filtered at: a) wavenumber 7, b) wavenumber 4, c) wavenumber 2. Contours at .005, .01, .02, .04, .08 m^2/sec^2 /spectral estimate in a) and .01, .02, .04, .08, .16, .32 m^2/sec^2 /spectral estimate in b) and c).

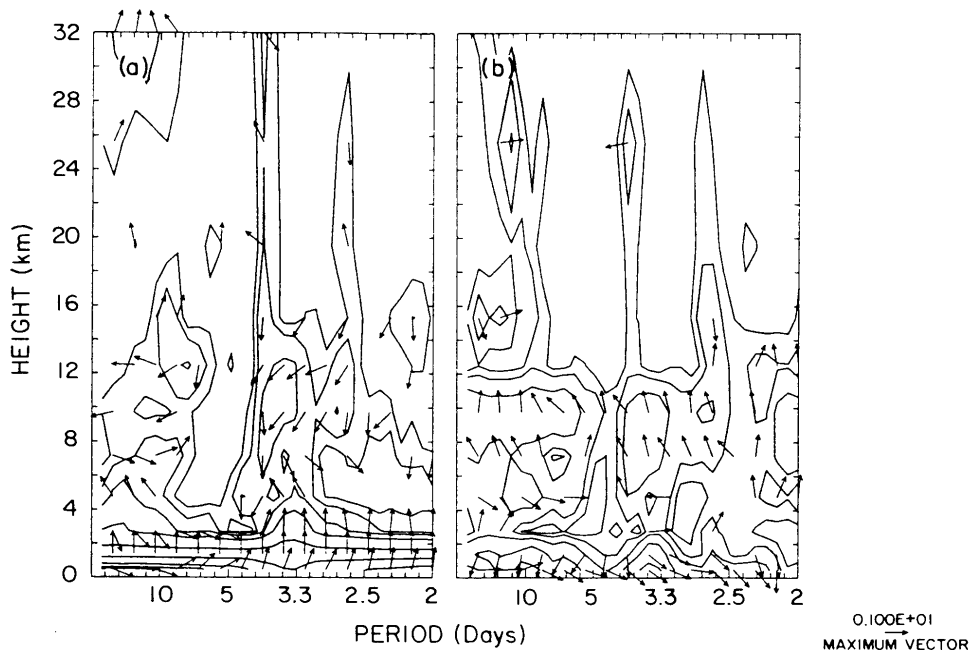


Fig. 9. Height versus period section of the coherence squared and phase between the symmetric meridional wind and the: a) symmetric meridional velocity at 811 mb and b) antisymmetric precipitation. Upwards pointing arrows mean the fields are in phase. An arrow pointing to the right (left) means the field leads (lags) the unfiltered meridional velocity by a quarter cycle. Contours at .05, .1, .2, .4, .8 in a) and .03, .06, .12, .24, .48 in b). The 95 % significance level is .1, computed as in Fig. 5.

the lower tropospheric and stratospheric responses. For wavenumber 7 there is essentially no stratospheric response at 3.6 days. We note that for both wavenumber 2 and wavenumber 4 the power increases rapidly with height above the region of heating.

Figure 9a (9b) shows the coherence squared between the 811 mb equatorially symmetric meridional velocity (the equatorially antisymmetric precipita-

tion) and the meridional velocity at all other levels. In each figure three wave "ducts" can be seen extending into the stratosphere. The upper tropospheric and lower stratospheric coherence peak near 3.6 days is clearly associated with lower tropospheric MRGWs and is related directly to the precipitation (Fig. 9b). Although the 3.6 day stratospheric signal is not statistically significant, its location and its phase agree with Figs. 2a and 6a. Additional analy-

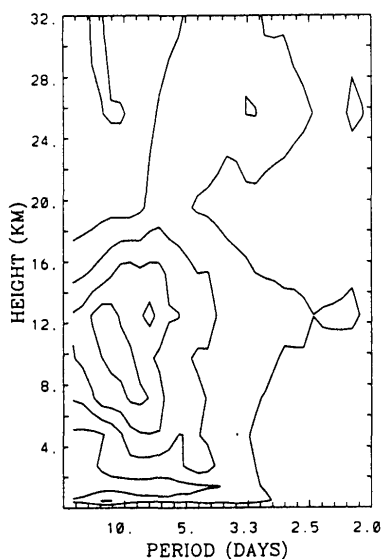


Fig. 10. As in Fig. 2a, but for the Kuo-Peq case.

sis (not shown) indicates that it is the wavenumber 2 and wavenumber 4 components of the 811 mb symmetric meridional velocity (the antisymmetric precipitation) which are coherent with the symmetric meridional velocity in the stratosphere at 3.6 days; wavenumber 7 does show much coherence between the troposphere and the stratosphere.

It is possible that the association of convection with the upper tropospheric waves is due to a downwards influence of the upper tropospheric signal. However, the hypothesis that both the upper tropospheric MRGWs and the lower tropospheric waves have a common source (namely convection) is strengthened by an additional integration, Kuo-Peq (see Table 1), in which the SST field is strongly distorted to have a sharp maximum on the equator. As a result only one ITCZ occurs, centered over the warmest SST on the equator. The vertical power distribution of the symmetric meridional velocity is shown in Fig. 10 for this case (compare with Fig. 2a). Slight hints of power maximum between 2.5 and 5 days in the lower troposphere and upper troposphere/lower stratosphere are indicated. A robust MRGW is not found in either the lower troposphere or the upper troposphere/lower stratosphere (substantiated by regression analysis, also see HBR). The equatorial zonal wind distribution in Kuo-Peq is very similar to that in the Kuo-Oct case (thus reducing possible differences in the MRGW signal due differences in the zonal wind distribution between the two cases). This suggests that the upper tropospheric disturbances are linked to those in the lower troposphere and to convective processes: without a robust lower tropospheric MRGW, a MRGW is not likely to be found in the upper troposphere in these model simulations.

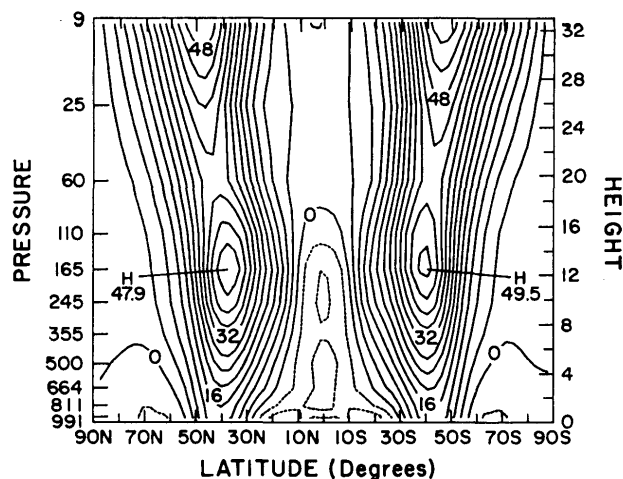


Fig. 11. The time (from day 20 to day 80) and zonally averaged distribution of zonal wind for the Kuo-Oct case. The contour interval is 4 m/sec.

3.2 Wavenumber selection due to the zonal mean wind

The discussion to follow implicitly assumes the WKBJ approach is valid. The condition for validity is that $mH_u \gg 2\pi$ (Andrews *et al.*, 1987), where H_u is the scale height on which the zonal mean wind varies and m is the vertical wavenumber ($m = 2\pi/L_z$, where L_z is the vertical wavelength). In the case of the rather weak vertical wind shear exhibited in the model equatorial regions this condition is approximately satisfied for MRGWs with periods of 3.6 days at the longer horizontal scales.

Assuming the WKBJ approach is valid, the small amplitude of the wavenumber 7 MRGW mode above the heating, as well as the behaviour of the wavenumber 4 and wavenumber 2 modes, can be explained using the zonal mean wind profile for the Kuo-Oct case (Fig. 11) and the dispersion relationship for westward propagating MRGWs. With a zonal mean wind, $\bar{u}(z)$, which is only a function of height the dispersion relationship for westward propagating MRGWs can be written as (Andrews *et al.*, 1987):

$$m(z) = N(\beta + k(\omega - k\bar{u}(z)))/(\omega - k\bar{u}(z))^2 \quad (1)$$

Here $\omega = 2\pi/T$, where T is the wave period; $k = 2\pi/L_x$, where L_x is the horizontal wavelength; $\beta = 2\Omega/a$, where Ω is the earth's rotation rate and a is the earth's radius, and N is the buoyancy frequency. Figure 12 shows the relation between vertical wavenumber (m) and zonal wavenumber ($n = ka$) for westward propagating MRGWs of various periods (T) assuming three different zonal mean wind values. The 3.6 day curve has been highlighted.

We note from Fig. 12, that for a mode at fixed period, the vertical wavelength can become infi-

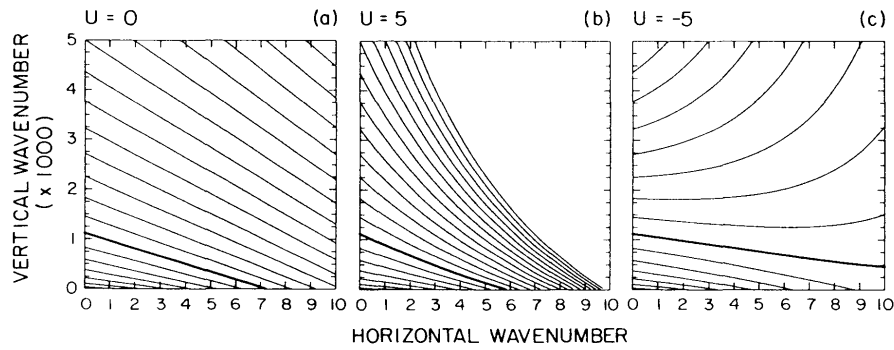


Fig. 12. The vertical wavenumber ($\times 1000$) (m^{-1}) versus the horizontal wavenumber at lines of constant absolute period for the MRGW. The period increases by .5 days, from 1.1 days (in the lower left corner) to 10.1 days. The 3.6 day dispersion curve is bold. The buoyancy frequency is assumed to be $.02 s^{-1}$, although the vertical wavenumber scales with the buoyancy frequency. a) assuming no mean zonal wind; b) assuming a mean zonal wind of $+5 ms^{-1}$; c) assuming a zonal mean wind of $-5 ms^{-1}$.

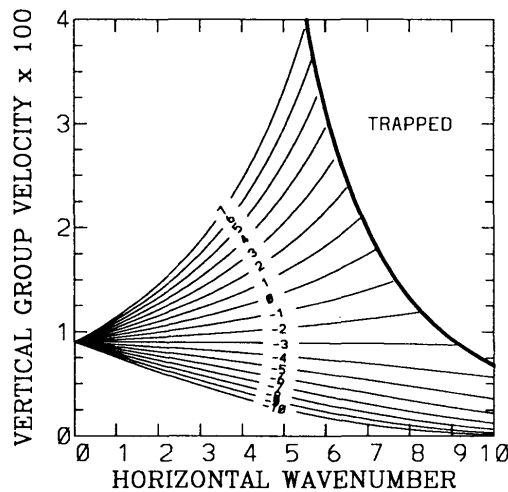


Fig. 13. The vertical group velocity ($\times 100$) (ms^{-1}) versus the horizontal wavenumber for a 3.6 day MRGW, assuming various mean zonal winds (from $-10 ms^{-1}$ to $7 ms^{-1}$). The region where the MRGW is trapped is demarcated by the heavy solid line.

nite ($m \rightarrow 0$) if the horizontal wavenumber is larger than a certain value, beyond which point the wave is evanescent. The criteria for the doppler shifted frequency of westward and vertically propagating MRGWs (see Eq. (1)) is:

$$\omega - uk > -\beta/k \tag{2}$$

where ω is specified to be negative for westward propagating waves, while k is positive. If the doppler shifted frequency decreases past this lower limit vertical propagation is prohibited. This criterion is similar to the Charney-Drazin criterion for vertically propagating Rossby waves (e.g. Andrews *et al.*, 1987). Therefore, as the zonal mean westerlies

are increased westward propagating MRGWs are doppler shifted towards more negative frequencies so that higher zonal wavenumber and longer period waves (*i.e.*, waves with small phase velocity) become trapped (Fig. 12b; also see Fig. 13). Figure 12a indicates that even with a zonal wind speed of zero, at 3.6 days wavenumber 7 is just external; thus, very weak westerlies are sufficient to prevent the vertical propagation of wavenumbers greater than 7 with periods of 3.6 days and longer. At 12 km the zonal winds are less than $-8 m/s$, but they rapidly increase to weak westerlies in the model stratosphere. It is clear that a wavenumber 7 mode with a period of 3.6 days cannot propagate into the model stratosphere where weak westerlies predominate, consistent with the model solution.

The behaviour of the wavenumber 2 and wavenumber 4 MRGWs in the model can be qualitatively explained by the fact that the vertical wavelength and vertical group velocity of MRGWs act to determine their spectrum. As their vertical wavelength and vertical group velocity decrease MRGWs become susceptible to radiative dissipation. Simple ray tracing theory (e.g. Andrews *et al.*, 1987) indicates that in a stationary zonal flow, it is the vertical wavenumber and vertical group velocity of a wave which changes with height in response to zonal wind shear, while the period and zonal wavenumber remain fixed (see Eq. (1)).

For a MRGW mode at fixed period the variation of the vertical group velocity ($\partial\omega/\partial m$) with respect to horizontal wavenumber and zonal wind can be determined from the gradient of T in Fig. 12. Fig. 13 summarizes this information for a MRGW with a period of 3.6 days. In the upper right hand corner of this figure, separated by the heavy solid line, no vertical group velocity is shown as it is in this region that the MRGW cannot propagate vertically. As the zonal mean wind decreases the vertical wave-

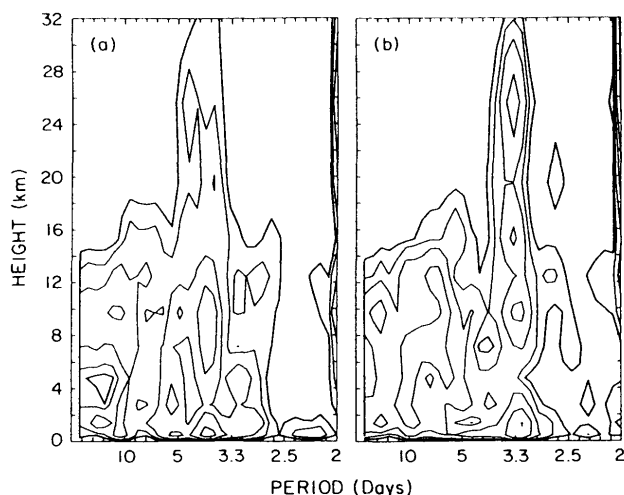


Fig. 14. As in Fig. 8b and 8c, but the power has been weighted by $e^{z/H}$. The contour interval used is: .00125, .0025, .005, .01, .02, .04, .08 $m^2/sec^2/spectral\ estimate$.

length (Fig. 12) and group velocity (Fig. 13) of a MRGW decreases for a wave at fixed period, leading to increased absorption of the wave mode. When the zonal mean wind is less than about $-3\ ms^{-1}$ MRGW modes with the largest zonal wavelengths are favored to propagate vertically under the influence of dissipation, as they have the largest group velocities. Holton (1972), in a modeling study of heat sources in the tropics, finds an antisymmetric heat source excites a wide range of wavenumbers (0-5), but only wavenumbers 2-4 propagate very far into the stratosphere when the stratospheric winds are easterly below 25 km. Boville and Randel (1992) show in a modeling study that the zonal wavelengths of MRGWs appear to increase with height in the stratosphere when the mean stratospheric winds are easterly, due to the selective absorption of modes with shorter length scales.

As zonal mean westerlies increase, the vertical wavelength and the vertical group velocity of MRGWs increase, primarily at the higher wavenumbers. This favors upwards propagation. However, in westerly mean winds the shorter horizontal wave modes are prohibited by Eq. (2). With westerly winds of $18\ ms^{-1}$ at 25 km Holton (1974) shows no MRGWs exist in the stratosphere; moderate zonal westerlies will tend to favor the intermediate scale waves.

The response of the wavenumber 2 and wavenumber 4 MRGW modes above the heating is qualitatively consistent with that expected from an examination of Fig. 12 and Fig. 13. Near 10 km the power of the symmetric meridional wind near 3.6 days is slightly larger, or about the same, at wavenumber

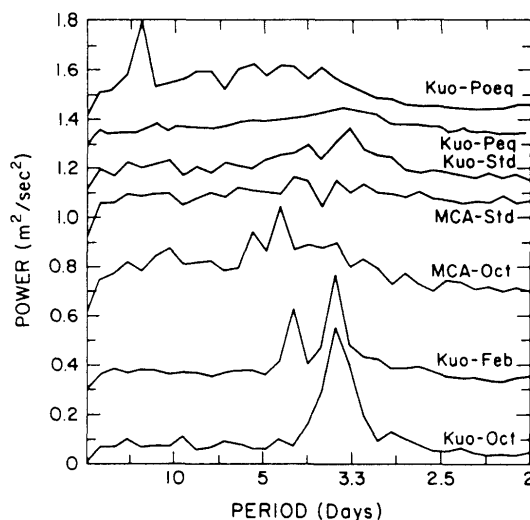


Fig. 15. The power spectra for the equatorial symmetric meridional velocity at 811 mb for the seven cases enumerated in Table 1. The spectra have been offset in each case to make them visible. In each case the base point (at zero period) has no power. The spectra are based on a 64 day time series. The units are $m^2/sec^2/spectral\ estimate$.

4 as at wavenumber 2^3 (Fig. 8). Assuming no dissipation of these wave modes above the tropopause, power will increase above the tropopause as $e^{z/H}$, where H is the scale height. Figure 14 shows the power of the wavenumber 2 and wavenumber 4 modes weighted by $e^{z/H}$ for the Kuo-Oct case. In the upper troposphere the weighted power of wave number 4 dissipates somewhat, but then stays relatively constant above the tropopause, decreasing by only a factor of two between 14 and 32 km. Wavenumber 2, on the other hand, shows very little decrease in its weighted power until 25 km, when the power suddenly decreases by over a factor of 4 in 7 km. In the upper troposphere (dominated by strong easterlies) wavenumber 4 dissipates faster than wavenumber 2 (as its group velocity is slower), while the opposite is true in the upper reaches of the model, dominated by weak westerlies.

Zonal winds in the lower equatorially stratosphere regularly switch between the easterly and westerly directions (the stratospheric QBO). Depending on the zonal wind direction and speed the smaller wavenumber MRGWs may be observed in the stratosphere. However, it is evidently very diffi-

³From Fig. 12a the vertical wavelength of wavenumber 4 is calculated to be 13 km, while that of wavenumber 2 is 8 km (assuming a buoyancy frequency of $.02\ s^{-1}$ and a period of 3.6 days). If the maximum response to heating occurs at twice the depth of the heating (Gill, 1980; Geisler and Stevens, 1981) then the heating will project more strongly on wavenumber 4 than wavenumber 2.

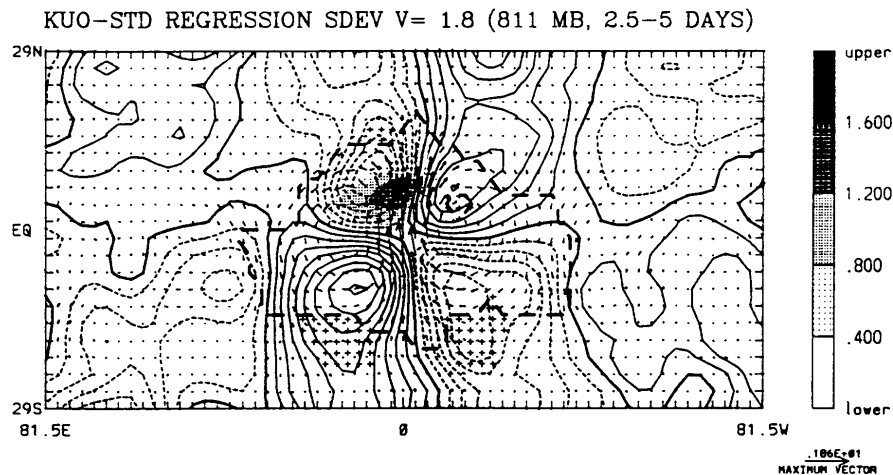


Fig. 16. As in Fig. 5, but for the Kuo-Std case and with a contour interval for the geopotential height of .1 m. All fields are scaled to the standard deviation of the meridional wind symmetric about the equator: 1.8 ms^{-1} .

cult for a wave with zonal wave number greater than 7 to be the dominant mode above the tropopause in either the easterly or westerly wind regime. When the zonal mean wind is westerly this wave mode is trapped because its doppler shifted frequency has become too negative (2); when vertical propagation is allowed in stratospheric easterlies, the vertical group velocity of this higher wavenumber MRGW modes is too slow to favor a strong response.

The peak in the power of the meridional wind at 811 mb (Fig. 3a) corresponds to the expected peak for an external mode of wavenumber 7 and period of 3.6 days in zero mean flow. As this mode has its maximum density weighted amplitude in the lowest model levels it may be the mode most strongly excited by CISK. The longer MRGW modes propagate out of the region of convective excitation and are most evident in the model stratosphere.

4. Sensitivity of the MRGW to convection

In this section we discuss the sensitivity of MRGWs to convective processes within the CCM1. We examine the MRGW at 811 mb for the cases listed in Table 1. We discuss the sensitivity of MRGWs to the convective scheme used and to the location of the mean convection.

The power spectra of the symmetric meridional wind on the equator is shown for the various experiments in Fig. 15 at 811 mb. The Kuo-Oct and Kuo-Feb cases show strong peaks in the power spectrum near 3.6 days. These cases also show pronounced MRGWs in the regression analyses (not shown for Kuo-Feb). The Kuo-Std case also exhibits a peak in the equatorial meridional wind between 2.5 and 5 days (albeit weaker). A regression analyses does indicate the presence of a MRGW (Fig. 16) in Kuo-Std. Note the wind and geopotential fields are all

significant in the vicinity of the regressed longitude.

In the Kuo-Oct, Kuo-Std and Kuo-Feb cases two ITCZs straddle the equator, consistent with the hypothesis that pronounced MRGWs are coincident with a split ITCZ (see Table 1). The strong MRGW observed in the regression analysis of the Kuo-Feb case and the coincident strong peak in the symmetric meridional wind spectrum between 2.5 and 5 days is not consistent with the results of HL: the observed MRGW mode is rather weak during the winter season. However, we note that the model with Kuo parameterized convection produces two ITCZs when forced with a February-like SST (although one ITCZ has about 50 % more rainfall than the other).

One off-equatorial ITCZ is obtained with the Kuo scheme by introducing sharp gradients into the equatorial SST distribution (Kuo-Poeq, Kuo-Peq) (see, HBR). A regression about the symmetric meridional wind for the Kuo-Poeq case (Fig. 17) demonstrates that energy in the 2.5 to 5 day band associated with cross equatorial flow is not due to MRGWs. The Kuo-Peq case (Fig. 18) does indicate equatorially trapped synoptic disturbances, but they are distorted compared with the theoretical MRGW.

Regression analysis is also performed for the disturbances associated with 2.5 to 5 day cross equatorial flow using the "October" SST distribution and the moist convective adjustment scheme (MCA-Oct). In this run the model produces two ITCZs. The regression analysis is shown in Fig. 19. The disturbance resembles that of a MRGW, but is not as longitudinally coherent as that in the Kuo-Oct case (Fig. 5) and only a portion of it is significant at the 95 % level. The moist convective adjustment case produces only one ITCZ on the equator when the standard sea surface temperature profile is

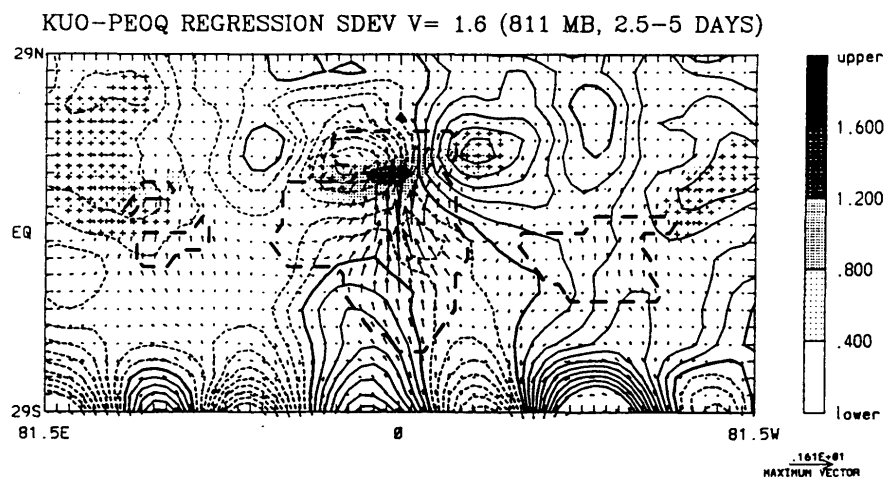


Fig. 17. As in Fig. 16, but for Kuo-Poeq case. All fields are scaled to the standard deviation of the meridional wind symmetric about the equator: 1.6 ms^{-1} .

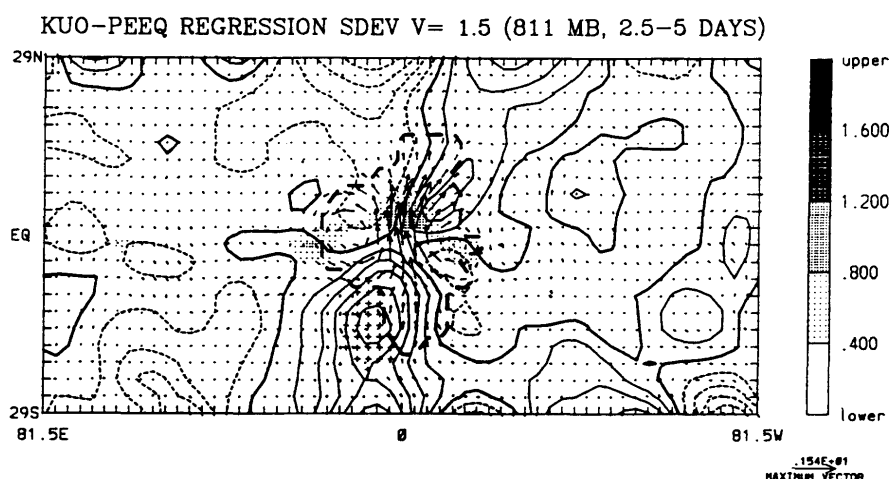


Fig. 18. As in Fig. 16, but for Kuo-Peeq case. All fields are scaled to the standard deviation of the meridional wind symmetric about the equator: 1.5 ms^{-1} .

used. The regression analysis for the MCA-Std case shows no indication of MRGWs (Fig. 20). Instead the regression depicts a simple down gradient flow of the meridional wind field across the equator correlated with very high rainfall amounts in the northern hemisphere. Thus, using the same SST profile (the standard profile) the moist convective adjustment scheme produces one ITCZ on the equator and no evidence of a MRGW, while the Kuo scheme produces a split ITCZ and a MRGW (also see HBR).

5. Discussion and conclusions

We have run a number of experiments with a GCM to examine the modeled structure of MRGWs. This model is run as an aqua planet. The aqua planet configuration allows a clear-cut relationship to be found between the SST and the wave modes generated. In addition, due to the zonal symmetry

of the model's lower boundary condition, it allows for a large number of degrees of freedom in a rather short model run.

Both the Kuo and MCA convective schemes give the most robust MRGW signal when the SST is such that the convective dynamics favor precipitation to occur on both sides of the equator (*i.e.*, a double ITCZ occurs). The SST distribution necessary to produce a double ITCZ depends on the convective scheme used, however (see HBR). In accordance with this, the definitive presence of MRGWs occur when the "Oct", "Feb" and "Std" SST distributions are used with the Kuo convective parameterization; with the MCA scheme it is only the "Oct" SST distribution which clearly shows a MRGW. The Kuo-Peeq experiment and the Kuo-Poeq experiment, each with sharply peaked SST distributions and only one ITCZ, do not indicate the presence of MRGWs.

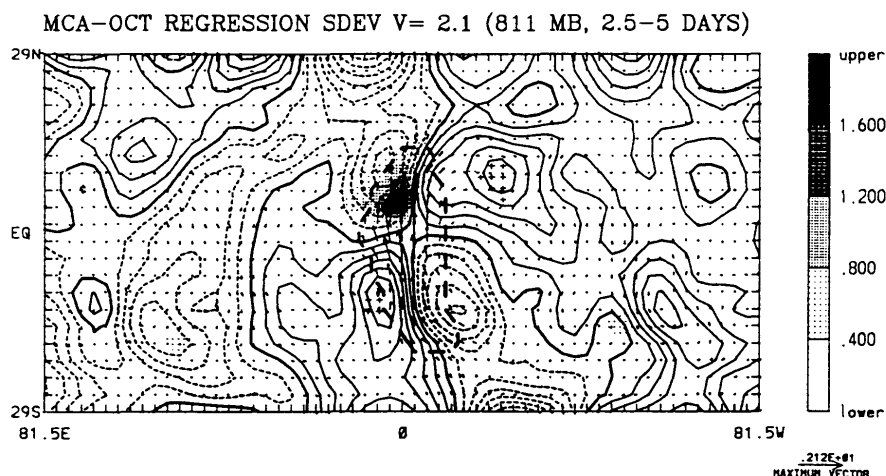


Fig. 19. As in Fig. 16, but for MCA-Oct case. All fields are scaled to the standard deviation of the meridional wind symmetric about the equator: 2.1 ms^{-1} .

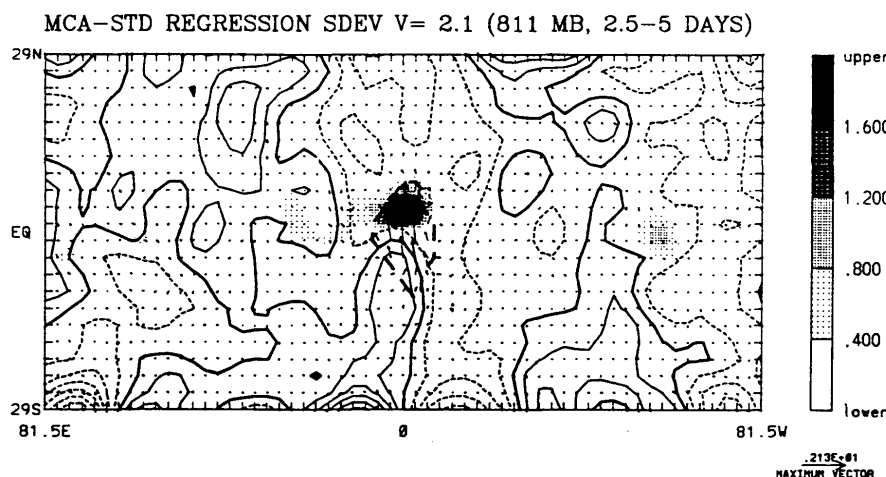


Fig. 20. As in Fig. 16, but for MCA-Std case. All fields are scaled to the standard deviation of the meridional wind symmetric about the equator: 2.1 ms^{-1} .

Neither does the MCA-Std case with one ITCZ located on the equator. Although the wave structure and climate of GCMs is very sensitive to the convective parameterization scheme used (HBR) both convective schemes tie MRGWs to SST distributions favoring convection on both sides of the equator. This suggests that the link between SST, double ITCZs and MRGWs is probably not an artifact of the convective scheme used. These results are consistent with the hypothesis that lower tropospheric MRGWs are primarily observed in the boreal fall season in the central Pacific due to the warm SSTs straddling the equator and the associated presence of a double ITCZ.

In a linear model in which the heating distribution is specified and does not interact with the resulting circulation one can demonstrate that it is the spatial and temporal distribution of heating which

generates MRGWs (Holton, 1972; SG). If stochastic convection is favored on both sides of the equator the projection of the heating onto MRGWs will be fairly robust because a portion of the heating will be antisymmetric about the equator. However, the response generated by the heating in a GCM is nonlinear: the MRGWs generated by the heating will in turn modulate the precipitation (and heating fields) and the static stability of the atmosphere. In addition, instabilities in the wave modes generated by the heating may greatly modify the structure and propagation characteristics of the waves themselves. This will in turn further modify the heating field. The results presented here suggest that the MRGW modes observed in the CCM1 are due to the interaction of CISK instability mechanisms and free-mode equatorial dynamics.

Precipitation in the model (see HBR) and the

ISCCP cloud brightness (not shown) both have a fairly white time spectrum within the ITCZ, implying that many different modes contribute to the rainfall within the ITCZ. However, when there is a double ITCZ a significant portion of the rainfall within the model, as well as the observed OLR, can be explained by the existence of MRGWs. Thus, it is very difficult to decouple the existence of two ITCZs from the existence of MRGWs, as the MRGWs contribute to the existence of the double ITCZ: both phenomena appear to occur simultaneously.

The detectable presence and strength of MRGWs in these runs depends on a subtle interaction between the parameterized convective scheme and the SST distribution. All the cases examined show a clear westward propagation of the meridional wind on the equator with a period between 2.5 and 5 days in Hoffmüller plots (not shown). However, not all the westward propagating wave modes are MRGWs; the regression analysis indicates that the Kuo-Poeq and MCA-Std runs do not contain a readily identifiable MRGW signal (see Fig. 18 and 20). Only in three cases, each with a double ITCZ climatology, does the power of the equatorial meridional wind stand out above the background noise between 2.5 and 5 days: the Kuo-Oct case, the Kuo-Feb case and the Kuo-Std case. The Kuo-Oct run with high SST under both convective branches of the ITCZ produces the strongest MRGW signal; the Kuo-Feb case with very high SST under one of the ITCZs, but significantly lower SST under the other ITCZ produces a signal almost as robust. The Kuo-Std case, with relatively low values of SST under both ITCZs produces a diminished spectral peak in the meridional component of wind on the equator, when compared with the Kuo-Oct case⁴. The convective scheme is also clearly important in determining the strength of the MRGW. For example, the MCA-Oct and Kuo-Oct runs differ only in the convective scheme used, but the Kuo-Oct run produces a much more pronounced MRGW (see Fig. 5 and Fig. 19). This is true despite the fact that both these runs produce off-equatorial ITCZs. In two runs with identical SSTs, the Kuo-Std and MCA-Std runs, only the Kuo-Std run produces identifiable MRGWs as it is the Kuo-Std run which has two ITCZs straddling the equator.

The fact that the Kuo convective scheme gives a much stronger and more coherent wave signal than the moist convective adjustment scheme suggests the importance of the CISK mechanism in producing a vigorous MRGW response in the model. Since

⁴Surprisingly, the relationship between SST and the MRGW signal does not appear to be entirely through the amount of rainfall associated with the MRGW (and consequently the amount of heating). The Kuo-Feb and Kuo-Std runs have comparable rainfall amounts in the ITCZ and yet the Kuo-Feb run produces a much stronger MRGW. This suggests the possible importance of evaporative processes.

convection in the model with the Kuo scheme is triggered almost exclusively by boundary layer moisture convergence (HBR), waves associated with convection should be pronounced in a model using this scheme. The fact that the most energetic MRGW is produced when the warmest water is coincident with the latitude of maximum low level convergence in the Kuo scheme also suggests the importance of instabilities in amplifying the MRGW: the coincidence of warm water and heating produces favorable energetics for the growth of this wave. Hayashi (1970) shows that unstable MRGWs tilt towards the northeast in the N.H., in agreement with the results obtained with the Kuo scheme (see, Figs. 5 and 16) and also in agreement with the observed structure of MRGWs (see LH). The wave produced in the model with the MCA scheme (Fig. 19) does not show much phase tilt in the horizontal plane.

Changes in the strength of the MRGW can also be due to changes in the vertical depth, spatial and time scales of the heating using different convective parameterizations. SG demonstrate the amplitude of a given wave mode depends on a matching between the three dimensional structure of the heating and the wave structure. Whereas the Kuo convective parameterization tends to heat the total atmospheric column, MCA tends to adjust (and to heat) three levels at a time. Thus, the heating in the MCA experiments tends to be shallower and more sporadic than in the Kuo experiments.

These experiments suggest a relationship between the MRGW mode observed in the upper troposphere and the mode maximizing in the lower troposphere. MRGWs appear to be forced on many spatial scales in the lower troposphere. As all these modes have approximately the same period, the phase speed of the longer modes is much faster than those with the shorter length scales. In the lower troposphere the shorter wavelength components dominate the spectrum and appear to be the most closely related to the heating and precipitation fields. The short scale modes disappear in the upper troposphere and lower stratosphere leaving the longer length scale waves to dominate the spectrum above the tropopause. Dunkerton (1993), in an analysis of equatorial radiosonde data from the Pacific basin, also finds a wave mode with largest amplitude in the lower troposphere and a baroclinic lower tropospheric structure, coupled to a longer mode in the upper troposphere and a stratospheric "tail". In agreement with HL this mode is observed primarily in the boreal fall season in the central Pacific.

We find the behaviour of the various MRGW modes above the heating agree very well with theory: above about 15 km wavenumber 7 is not visible as it is doppler shifted beyond the "Charney-Drazin" cut-off frequency (2) and is thus trapped in the lower troposphere. Wavenumber 4 shows relatively little

dissipation in the stratospheric westerlies (compared to wavenumber 2) as its vertical group velocity becomes relatively large in westerly winds.

The results discussed above concerning wavenumbers 2 and 4 must be treated with some caution. Although a zonally symmetric aqua planet simulation may be thought to represent the Pacific basin, on longer spatial scales zonal asymmetries may become important. In addition, these experiments are carried out at coarse stratospheric resolution which may influence the propagation characteristics of these wave modes above the tropopause. Boville and Randel (1992) show, however, that inadequate vertical resolution can actually enhance the vertical propagation of MRGWs.

These experiments suggest that the forcing mechanism for 2.5–5 day MRGWs in the troposphere is the spatial distribution of the SST in the central Pacific. We show a connection between the waves observed in the upper troposphere/lower stratosphere with the MRGW maximizing near the surface and associated with convection. Our results suggest that the observed Yanai wave and the lower tropospheric MRGWs documented by HL are explicitly related. The possibility cannot be altogether dismissed that lateral forcing (*cf.* Itoh and Ghil, 1988), or other forcing mechanisms may be important in forcing MRGWs above the tropopause at different times of year and under different zonal wind distributions than found in the model. However, in this study, we find no evidence that the 2.5–5 day MRGWs in the lower stratosphere are forced independently from those in the lower troposphere. The implication is that the activity of MRGWs in the stratosphere will be enhanced during certain times of year and over certain locations.

Acknowledgements

This work was supported by the National Center for Atmospheric Research, NASA grant NAGW-1138 (HH) and the National Science Foundation (DSB; grant ATM 8822980). We would like to thank Brant Liebmann and two anonymous reviewers for their help.

References

- Andrews, D.G., J.R. Holton and C.B. Leovy, 1987: *Middle Atmosphere Dynamics*, Academic Press Inc., 489 pp.
- Anthes, R.A., 1977: A cumulus parameterization scheme utilizing a one-dimensional cloud model. *Mon. Wea. Rev.*, **105**, 270–286.
- Boville, B.A., W.J. Randel, 1992: Equatorial waves in a stratospheric GCM: effects of vertical resolution. *J. Atmos. Sci.*, **49**, 755–801.
- Deardorff, J.W., 1972: Parameterization of the planetary boundary layer for use in a general circulation model. *Mon. Wea. Rev.*, **100**, 93–106.
- Donner, L.J., H.-L. Kuo and E.J. Pitcher, 1982: The significance of thermodynamic forcing by cumulus convection in a general circulation model. *J. Atmos. Sci.*, **39**, 2159–81.
- Donner, L.J., 1986: Sensitivity of the thermal balance in a general circulation model to a parameterization for cumulus convection with radiatively interactive clouds. *J. Atmos. Sci.*, **43**, 2277–88.
- Dunkerton, T.J., 1993: Observation of 3–6 day meridional wind oscillations over the tropical Pacific, 1973–1992: vertical structure and interannual variability. Submitted to, *J. Atmos. Sci.*
- Hayashi, Y., 1970: A theory of large-scale equatorial waves generated by condensation heat and accelerating the zonal wind. *J. Meteorol. Soc. Japan.*, **48**, 140–160.
- Hayashi, Y., 1974: Spectral analysis of tropical disturbances appearing in a GFDL general circulation model. *J. Atmos. Sci.*, **31**, 180–218.
- Hendon, H.H. and B. Liebmann, 1991: The structure and annual variation of antisymmetric fluctuations of tropical convection and their association with Rossby-gravity waves. *J. Atmos. Sci.*, **48**, 2127–2140.
- Hess, P., D.S. Battisti and P. Rasch, 1993: The maintenance of the intertropical convergence zones and the large-scale tropical circulation on a water covered earth. *J. Atmos. Sci.*, **50**, 691–713.
- Holton, J.R., J.M. Wallace and J.A. Young, 1971: On boundary layer dynamics and the ITCZ. *J. Atmos. Sci.*, **28**, 275–280.
- Holton, J.R., 1972: Waves in the equatorial stratosphere generated by tropospheric heat sources. *J. Atmos. Sci.*, **29**, 368–375. 585–604.
- Holton, J.R. and R.S. Lindzen, 1972: An updated theory for the quasi-biennial cycle of the tropical stratosphere. *J. Atmos. Sci.*, **29**, 1076–1080.
- Itoh, H. and M. Ghil, 1988: The generation mechanism of mixed Rossby-gravity waves in the equatorial troposphere. *J. Atmos. Sci.*, **45**, 585–604.
- Krishnamurti, T.N., S. Low-Nam and R. Pasch, 1983: Cumulus parameterization and rainfall rates II. *Mon. Wea. Rev.*, **111**, 815–828.
- Kuo, H.L., 1965: On formation and intensification of tropical cyclones through latent heat release by cumulus convection. *J. Atmos. Sci.*, **22**, 40–63.
- Kuo, H.L., 1974: Further studies of the parameterization of the influence of cumulus convection of large-scale flow. *J. Atmos. Sci.*, **31**, 1232–40.
- Kuo, H.L., 1975: Instability theory of large-scale disturbances in the tropics. *J. Atmos. Sci.*, **32**, 2229–2245.
- Liebmann, B.L. and H.H. Hendon, 1990: Synoptic-scale disturbances near the equator. *J. Atmos. Sci.*, **47**, 1463–1479.
- Lindzen, R.S. and J.R. Holton, 1968: A theory of the quasi-biennial oscillation. *J. Atmos. Sci.*, **30**, 1095–1107.
- Manabe, S.J. Smagorinsky and R.F. Strickler, 1965: Simulated climatology of a general circulation model with a hydrologic cycle. *Mon. Wea. Rev.*, **93**, 769–799.
- Matsuno, T., 1966: Quasi-geostrophic motions in the equatorial area. *J. Meteor. Soc. Japan*, **44**, 25–42.

- Murakami, M., 1979: Large-scale aspects of deep convective activity over the GATE area. *Mon. Wea. Rev.*, **107**, 994–1013.
- Nitta, T., 1970: Statistical study of tropospheric wave disturbances in the tropics Pacific region. *J. Meteor. Soc. Japan*, **48**, 47–59.
- Randel, W.J., 1992: Upper tropospheric equatorial waves in ECMWF analyses. *Quart. J. Roy. Meteor. Soc.*, **118**, 365–394.
- Reed, R.J. and E.E. Recker, 1971: The structure and properties of African wave disturbances as observed during Phase III of GATE. *Mon. Wea. Rev.*, **105**, 317–333.
- Salby, M.L. and R.R. Garcia, 1987: Transient response to localized episodic heating in the tropics. Part I: Excitation and short-time near-field behavior. *J. Atmos. Sci.*, **44**, 458–498.
- Salby, M.L., H.H. Hendon, K. Woodberry and K. Tanaka, 1991: Analysis of global cloud imagery from multiple satellites. *Bull. Amer. Meteor. Soc.*, **72**, 467–480.
- Wallace, J.M., 1971: Spectral studies of tropospheric wave disturbances in the tropical western Pacific. *Rev. Geophys. Space Phys.*, **9**, 557–612.
- Williamson, D.L., J.T. Kiehl, V. Ramanathan, R.E. Dickinson and J.J. Hack, 1987: Description of NCAR Community Climate Model (CCM1). NCAR Tech. Note, NCAR/TN-285+STR, National Center for Atmospheric Research, Boulder, CO NTIS PB87-203782/AS, 112 pp.
- Yanai, M. and T. Maruyama, 1966: Stratospheric wave disturbances propagating over the equatorial Pacific. *J. Meteor. Soc. Japan*, **44**, 291–294.
- Yanai, M. and T. Maruyama, 1970: A further study of tropical wave disturbances by the use of spectrum analysis. *J. Meteor. Soc. Japan*, **48**, 185–197.
- Zangvil, A. and M. Yanai, 1981: Upper tropospheric waves in the tropics. Part II: Association with clouds in the wavenumber-frequency domain. *J. Atmos. Sci.*, **38**, 939–953.

大気大循環モデルに現れた混合ロスビー・重力波と対流との関係

Peter G. Hess

(米国大気研究センター)

Harry H. Hendon

(米国コロラド大学大気理論・解析センター)

David S. Battisti

(ワシントン大学大気科学教室)

大気大循環モデルで再現された混合ロスビー・重力波 (MRGW) と対流との関係を調べた。下層の境界条件として全領域で海洋を与えた大気大循環モデルを用いて数値実験を行った。対流のパラメタリゼーションの方式 (修正した Kuo 方式と対流調節法) や熱帯の海面水温 (東西方向には一様) を変えて幾つかの数値実験を行った。その結果、実験毎に ITCZ (熱帯収束帯) の位置が変化することがわかった。赤道を挟んで2つの ITCZ が存在するような海面水温分布を与えた時、活発な MRGW が現れる。モデルに現れた MRGW の構造や強さは、海面水温分布や対流のパラメタリゼーションに左右される。MRGW が最も活発な実験の時の波の垂直構造を調べた。その結果、対流圏中・下層では対流活動に呼応して異なった東西スケールを持った幾つかの MRGW が存在するが、上部対流圏や下部成層圏では長い波長の波しか存在しないことがわかった。